HHS Public Access

Author manuscript

Neurobiol Aging. Author manuscript; available in PMC 2017 February 01.

Published in final edited form as:

Neurobiol Aging. 2016 February ; 38: 104–111. doi:10.1016/j.neurobiolaging.2015.10.025.

Local and distributed PiB accumulation associated with development of preclinical Alzheimer's disease

Matthew R. Brier[a], **John E. McCarthy**[b], **Tammie L.S. Benzinger**[c,d], **Ari Stern**[b], **Yi Su**[c], **Karl A. Friedrichsen**[c], **John C. Morris**[a,d], **Beau M. Ances**[a,c,d,*,1], and **Andrei G. Vlassenko**[c,d,1]

[a]Department of Neurology, Washington University School of Medicine, St. Louis, MO, USA

[b]Department of Mathematics, Washington University School of Medicine, St. Louis, MO, USA

[c]Department of Radiology, Washington University School of Medicine, St. Louis, MO, USA

[d]The Knight Alzheimer Disease Research Center, Washington University School of Medicine, St. Louis, MO, USA

Abstract

Amyloid-beta plaques are a hallmark of Alzheimer's disease (AD) that can be assessed by amyloid imaging (e.g., Pittsburgh B compound [PiB]) and summarized as a scalar value. Summary values may have clinical utility but are an average over many regions of interest, potentially obscuring important topography. This study investigates the longitudinal evolution of amyloid topographies in cognitively normal older adults who had normal (N = 131) or abnormal (N = 26) PiB scans at baseline. At 3 years follow-up, 16 participants with a previously normal PiB scan had conversion to PiB scans consistent with preclinical AD. We investigated the multivariate relationship (canonical correlation) between baseline and follow-up PiB topographies. Furthermore, we used penalized regression to investigate the added information derived from PiB topography compared to summary measures. PiB accumulation can be local, that is, a topography predicting the same topography in the future, and/or distributed, that is, one topography predicting another. Both local and distributed PiB accumulation was associated with conversion of PiB status. Additionally, elements of the multivariate topography, and not the commonly used summary scalar, correlated with future PiB changes. Consideration of the entire multivariate PiB topography provides additional information regarding the development of amyloid-beta pathology in very early preclinical AD.

Keywords

Multivariate statistics; Canonical correlation; Lasso; Amyloid beta

[*]Corresponding author at: Department of Neurology, School of Medicine, Washington University, 660 S Euclid, St Louis, MO 63110, USA. Tel.: 314 747 8423 fax: 314 747 8427. ancesb@neuro.wustl.edu (B.M. Ances).

[1]Contributed equally.

Disclosure statement

The authors report no conflict of interest. This study was funded by the NIH as specified in the acknowledgements.

1. Introduction

Alzheimer's disease (AD) is characterized by a long preclinical period wherein pathology accumulates in the absence of overt symptoms (Price et al., 2009). The deposition of amyloid-beta (Aβ), measured via positron emission tomography (PET) using Pittsburgh compound B (PiB) (Klunk et al., 2004), is one of the earliest measurable pathological changes in AD (Braak and Del Tredici, 2012; Jack et al., 2013) and can be monitored longitudinally (Sojkova et al., 2011; Villemagne et al., 2011; Vlassenko et al., 2011). The results of PiB scans are often summarized into a single scalar metric defined as an average over a group of regions known to accumulate the most of Aβ plaques in symptomatic AD. PiB scans assessed in this way are dichotomized as either PiB negative (PiB−) or PiB positive (PiB+) (Mintun et al., 2006). A PiB+ scan in a cognitively normal individual is interpreted as presumptive evidence for preclinical AD (Jack et al., 2012; Morris et al., 2014; Sperling et al., 2011) and predicts clinical progression (Morris et al., 2009). Dichotomizing PiB status is potentially clinically useful but reduces complex and potentially informative topographies to a single scalar metric.

The earliest detectably abnormal amyloid topography is relatively focal but becomes more expansive as the disease progresses (Braak et al., 2011; Thal et al., 2002). Understanding of this early topography, how it differs from the topography of the highest PiB retention at the more advanced stages of AD and how it progresses in the early stage of the disease remains unclear. Multivariate statistical techniques, well suited for examining local and distributed phenomena, may help to characterize better the relationships in longitudinal amyloid topographies as assessed by PiB.

In this study, we followed 157 cognitively normal participants who were PiB− (N = 131) or PiB+ (N = 26) at baseline as assessed by a summary scalar value of mean cortical (MC) standardized uptake value ratio (SUVR). These participants were followed longitudinally (mean follow-up: ~3 years). In participants who developed significant PiB accumulation (i.e., became PiB+), we investigated the topographic progression of PiB accumulation using canonical correlation. Canonical correlation identifies pairs of highly correlated topographies. We then compared the ability of the single scalar value and topographic measures to capture the underlying PiB accumulation associated with the development of preclinical AD.

2. Methods

2.1. Subjects

Participants were community dwelling volunteers (age range 45–85 years) enrolled in the Adult Children Study project at the Washington University in St Louis Knight Alzheimer Disease Research Center. All participants were cognitively normal, both at baseline and at follow-up PiB scans, as assessed by a Clinical Dementia Rating score of 0 (Morris, 1993) and the Mini-Mental Status Examination. Participants were in good general health with no neurological, psychiatric, or systemic medical illness that could disrupt longitudinal participation. Each participant underwent magnetic resonance imaging (MRI) and PiB PET (described in the following section). Baseline scans were dichotomized as either PiB− or

PiB+ (criteria described in the following section) and a second scan was performed on average 3.29 years later (standard deviation = 1.22 years; minimum = 0.96 years; maximum = 6.47 years). Participants were divided into 3 groups based on their PiB status at baseline and follow-up: CNnn (cognitively normal, PiB− at both scans, N = 115), CNnp (cognitively normal, PiB− at first scan but PiB+ at second scan, N = 16), or CNpp (cognitively normal, PiB+ at both scans, N = 26). Complete demographic information is shown in Table 1.

2.2. MRI assessment

MRI consisted of an magnetization-prepared rapid gradientecho T1-weighted image collected on a Siemens (Erlangen, Germany) MR scanner. Images are processed using FreeSurfer software version 5.1 (Martinos Center for Biomedical Imaging, Charlestown, MA, USA) (Fischl et al., 2002). All FreeSurfer parcelations were assessed for accuracy by a skilled investigator (Karl A. Friedrichsen). Only gray matter regions were included in this analysis.

2.3. PET assessment

The PiB PET assessment has been previously described in detail (Su et al., 2013, 2014). Imaging was conducted on a Siemens 962 HR+ ECAT PET scanner or a Siemens Biograph 40 scanner. PET data were analyzed using previously developed methods (Su et al., 2013, 2015). FreeSurfer segmentation (Fischl et al., 2002) (http://freesurfer.net/) was used as the basis for quantitative analysis to obtain regional SUVR with cerebellar gray matter serving as the reference region. Partial volume correction was also performed using a regional spread function technique (Rousset et al., 1998; Su et al., 2015).

PiB positivity was defined using the MC SUVR across the precuneus, prefrontal, gyrus rectus, and temporal FreeSurfer regions of interest (ROIs) (Morris et al., 2010). A cutoff value of 1.42 was used which is comparable to an MC binding potential of 0.18 that was previously defined (Mintun et al., 2006; Su et al., 2013). Characteristic SUVR images are presented in Fig. 1. The equivalence for an MC SUVR of 1.42 and MC-BP of 0.18 was previously determined using regression in an independent sample (unpublished data). Because of the criticality of this cutoff for subsequent analyses, primary results are also replicated using an alternative cutoff determined from this sample (Supplementary Material).

2.4. Canonical correlation analysis

We investigated the progression of PiB topography in CNnp, CNnn, and CNpp groups separately. To do this, we calculated the canonical correlation between the PiB topography at baseline and the PiB topography at follow-up using 42 ROIs (Hardle and Simar, 2007; Hotelling, 1936). A canonical correlation is the weighted average of variables (termed canonical variables) in one distribution that are maximally correlated with the weighted average of variables from another distribution. There can be multiple significant canonical correlations that isolate unique variance (similar to PCA components).

Let X_1, $X_2 \in \mathbb{R}^{N \times M}$ index the regional PiB SUVR in N subjects and M = 42 ROIs at time point 1 and 2, respectively. Define:

$$\sum = \begin{bmatrix} \sum_1 & \sum_{12} \\ \sum_{21} & \sum_2 \end{bmatrix} = \begin{bmatrix} X_1^T X_1 & X_1^T X_2 \\ X_2^T X_1 & X_2^T X_2 \end{bmatrix}$$

In this case, Σ is rank deficient which precludes matrix inversion. Therefore, define $\hat{\sum} = (1-\alpha)\sum + \alpha\Delta$, where α is an arbitrary parameter and Δ is a shrinkage target (Schafer and Strimmer, 2005). For this analysis, α is calculated in closed form as previously described (Ledoit and Wolf, 2003); Δ is defined as the diagonal matrix of Σ which ensures that $\hat{\sum}$ is full rank (Ledoit and Wolf, 2004). This approach was recently applied to analyze functional MRI data (Brier et al., 2015).

The number of significant canonical correlations is defined as the dimensionality of $\hat{\sum}_{12}$. Here, we estimate this dimensionality using an information criterion (Minka, 2000). For every significant canonical correlation there exist 2 canonical variables: one corresponding to the baseline PiB topography and another corresponding to the follow-up PiB topography. Let a_i be the ith canonical variable corresponding to the baseline PiB topography; a_i is defined as the ith eigenvector of $\hat{\sum}_1^{-1}\hat{\sum}_{12}\hat{\sum}_2^{-1}\hat{\sum}_{21}$. Similarly, let b_i be the ith canonical variable corresponding to the follow-up PiB topography; b_i is defined as the ith eigenvector of $\hat{\sum}_2^{-1}\hat{\sum}_{21}\hat{\sum}_1^{-1}\hat{\sum}_{12}$. The values of a_i and b_i are unit norm and maximize the correlation between $a_i^T X_1$ and $b_i^T X_2$.

2.5. Penalized regression

We fit an elastic net penalized regression model which uses the linear combination of an L_1 and L_2 norm of the calculated β values as a penalty (also known as least absolute shrinkage and selection operator [LASSO] and ridge regression, respectively) (Hastie et al., 2001; Tibshirani, 1996; Zou and Hastie, 2005). Penalized regression differs from ordinary least squares (OLS) regression in that it enforces a penalty term that forces some favorable property on the resulting regression βs. The L_1 penalty (LASSO) penalizes nonzero β values and thus forces small β values to 0 and retains a small number of nonzero β values. This results in a model that is more easily interpretable (i.e., has only a few terms to consider). However, in data that are highly colinear the decision to retain one variable and discard a highly correlated variable is arbitrary (Zou and Hastie, 2005). The elastic net accommodates this data feature by allowing highly correlated predictor variables to enter the model simultaneously. This flexibility is accomplished by relaxing the L_1 penalty with some fraction of an L_2 penalty.

We fit 2 separate elastic net models: The first uses follow-up MC SUVR as an outcome variable and the second uses percent change in MC SUVR as an outcome variable. Let $y = [y_1, y_2, \ldots, y_N] \in \mathbb{R}$ be the outcome variable of interest, either follow-up MC SUVR or the percent change in MC SUVR between baseline and follow-up. Furthermore, let $X = \mathbb{R}^{N \times [M+1]}$ index the regional PiB SUVR in N subjects and M = 40 ROIs. The M + first

region is the baseline MC SUVR value which is included to investigate its sufficiency as a predictor. All variables were mean centered and made unit variance (z-scored). The estimate of penalized regression coefficients then has the form:

$$\underset{\hat{\beta}}{arg\min}\|y - X\hat{\beta}\|^2 + \lambda\left((1-\alpha)\|\hat{\beta}\|^2 + \alpha\|\hat{\beta}\|_1\right)$$

The first term is OLS regression. The second and third terms are the L_2 and L_1 norms, respectively. λ determines the overall penalty severity and α determines the relative contribution of the L_1 and L_2 penalty. Both parameters are selected by leave-one-out cross validation.

To compare the power of baseline MC SUVR and the entire topography to predict follow-up MC SUVR or percentage change in MC SUVR we compared the adjusted-R^2 values:

$$adj\ R^2 = 1 - \frac{(1-R^2)(N-1)}{N - df - 1}$$

For OLS, the *df* is the number of predictors. Similarly, for LASSO regression the number of *df* is the number of nonzero β values. However, in elastic net regression the number of *df* is complicated by the potential for colinearity in the selected predictors. Thus, df is defined as:

$$df = Tr\left(X_{\mathscr{A}}\left(X_{\mathscr{A}}^T X_{\mathscr{A}} + (\lambda\cdot(1-\alpha))\,I\right)^{-1} X_{\mathscr{A}}^T\right)$$

where Tr indicates the trace and $\mathscr{A}$ indicates the active predictor set (Zou and Hastie, 2005).

3. Results

We first investigated the evolution of PiB topography in the CNnp group. The number of significant canonical correlations was determined to be 3 using an information criteria (Minka, 2000). The first canonical correlation was characterized by the baseline topography in Fig. 2A and the follow-up topography in Fig. 2B. The baseline topography was dominated by large positive weights in the posterior cingulate, precuneus, and superior temporal regions balanced by negative weights in lateral frontal regions. At follow-up the topography was similar but now also included inferior and lateral temporal regions. These topographies were highly correlated (Fig. 2C; r = 0.58, $p < 10^{-4}$). For example, the precuneus and temporal regions are positive in both topographies and lateral frontal regions are strongly negative. The original regional data are then projected onto these topographies yielding a single scalar value for each subject at baseline and follow-up. Put another way, the weighted average of PiB binding (weighted according to the loadings in the topographies) was calculated at baseline and follow-up. These baseline and follow-up scalar values were highly correlated (Fig. 2D; r = 0.99; $p < 10^{-10}$) with follow-up significantly higher. Thus, this canonical correlation represents the accumulation of Aβ locally in regions already affected.

The second canonical correlation, isolated after removing the variance related to the first canonical correlation, had a different pattern. The topographies of PiB for the baseline and follow-up scan are shown in Fig. 2E and F, respectively. The baseline topography was dominated by large positive weights in posterior cingulate, precuneus, and lateral parietal regions. In contrast, frontal regions dominated the follow-up topography. In contrast to the first canonical variable, the topographies were not as strongly correlated (Fig. 2G; r = 31; p= 0.04). This indicates that baseline PiB topography predicts PiB values in a different topography at follow-up. Projection of the original data onto these topographies resulted in a strong positive correlation (Fig. 2H; r = 0.99; $p < 10^{-10}$). The prediction of a distinct topography at follow-up based on a different topography at baseline suggests that this canonical correlation represents the expansion of Aβ topography to additional regions in the CNnp group.

The third canonical correlation has yet a different pattern. The topographies of PiB for the baseline and follow-up scan are shown in Fig. 2I and J and were moderately correlated (Fig. 2K; r = .47, p = 0.002). The baseline topography was dominated by the anterior cingulate, whereas the follow-up topography was dominated by precuneus and subcortical regions. Projection of the original data onto this topography resulted in a strong positive correlation (Fig. 2L; r = 0.99; $p < 10^{-10}$). This canonical correlation represents a combination of local and distributed processes distinct from the 2 aforementioned processes. These canonical correlation analyses were replicated using an alternative cutoff (Supplementary Material).

One analytic decision present in the previous results is the averaging of homotopic regions into a single bilateral ROI. We sought to determine whether this assumption (similar results on the left and right) was supported by the data. To accomplish this, the number of columns in X was doubled to 2M corresponding to left and right regional SUVR values being represented separately. The number of canonical correlations in this lateralized data set was determined to be 3 by an information criteria (Minka, 2000). This was the same number of canonical correlations identified in the homotopic analysis described previously. There were 2 critical analytic questions to be addressed: (1) were the topographies isolated in the lateralized analysis symmetric across the midsagittal plane and (2) were the same topographies isolated in the lateralized analysis similar to those in the homotopic analysis. To address the first question, within a single topography the loadings on the left were regressed onto the loadings on the right. For all topographies (3 canonical correlations with a baseline and follow-up topography) the left and right loadings were strongly related (all $p <$ 0.05). In each case, the 95% confidence intervals on the regression β crossed 1, suggesting equal values for the left and the right hemispheres. Nevertheless, the maximum likelihood β estimate favored a larger representation in the left hemisphere compared to the right hemisphere but this bias was not significant. We next examined whether the topographies isolated in the lateralized analysis were similar to the topographies isolated in the homotopic analysis. For each canonical correlation (both baseline and follow-up), the topography resulting from the homotopic analysis was highly correlated between the left and right (analyzed separately) hemisphere topographies resulting from the lateralized analysis (all r > 0.65; all $p < 0.001$). These data suggest a bias toward representation of the left hemisphere, but this difference does not lead to significantly different PiB accumulation with respect to hemisphere.

A single canonical correlation described the relationship between baseline and follow-up PiB topographies in the CNnn group (Fig. 3A and B). The baseline and follow-up topographies were not correlated (Fig. 3C) and did not demonstrate any obvious biological topography. Furthermore, the projected PiB values did not show systematic increases (Fig. 3D), indicating no accumulation, consistent with their CNnn status.

A single canonical correlation described the relationship between baseline and follow-up PiB topographies in the CNpp group (Fig. 4). The baseline topography (Fig. 3A) was not significantly correlated with the follow-up topography (Fig. 4B; r = 0.12, $p = 0.44$). However, the projected PiB values were strongly correlated (r = 0.99; $p < 10^{-10}$) and a dramatic accumulation was seen at follow-up, as reflected by data above the identity line (Fig. 4D). These results suggest that CNpp individual at baseline continues to have significant accumulation longitudinally.

We next turned to the question of defining the correlates of future PiB accumulation in those who were PiB− at baseline. Accepting that the MC SUVR is a reliable measure of the level of AD pathology, can follow-up values be understood as a function of the baseline scan? Across all subjects, the baseline and follow-up MC SUVR were highly correlated (r = 0.55, $p < 10^{-11}$, Adj-$R^2 = 0.30$) suggesting that, relative to the interindividual variance, MC SUVR values did not dramatically change over a period of 3 years. Importantly, only within just the CNnp group were the baseline and follow-up MC SUVR not correlated (r = 0.24, $p = 0.36$). Baseline MC SUVR was also not correlated with the percent change in MC SUVR across scans (r = 0.026, $p = 0.77$, Adj-$R^2 = -0.007$). A negative Adj-R^2 indicates poor model fit. Notably, the baseline MC SUVR and percent change in MC SUVR was negatively correlated in the CNpp group (r = −0.54, $p = 0.0047$), suggesting a slowing of PiB accumulation within this topography. Thus, an open question is what features in the baseline topography correlates with future change in MC SUVR.

To investigate which features of the baseline topography correlate with the follow-up MC SUVR and percent change in MC SUVR, we fit 2 separate elastic net models using individual regional SUVR values as predictors. The β coefficients corresponding to the minimum cross-validation error for each model are shown in Table 2 and depicted visually in Fig. 5. Positive values predict relatively higher MC SUVR or positive changes in MC SUVR in the first (predicting MC SUVR) and second model (predicting percent change in MC SUVR) and negative values predict relatively lower MC SUVR or negative changes in MC SUVR. Importantly, the baseline MC SUVR only entered the model for predicting follow-up MC SUVR and not for predicting the change in MC SUVR. The correlation between the predicted follow-up MC SUVR and the actual MC SUVR was significantly correlated (r = 0.73, $p < 10^{-22}$) and after correcting for the number of predictors was better than baseline MC SUVR alone (Adj-$R^2 = 0.50$ compared with 0.30). Similarly, the predicted percent change in MC SUVR was significantly correlated with the actual percent change in MC SUVR (r = 0.54, $p < 10^{-10}$) and, after correcting for the number of predictors, was better than baseline MC SUVR alone (Adj-$R^2 = 0.25$ compared with −0.007).

4. Discussion

This report uses two multivariate techniques (canonical correlation and penalized regression) to describe expanding Aβ topographies, as assessed by PiB, and identifies patterns of deposition correlated with future PiB accumulation. Canonical correlation finds topographies that represent local and distributed accumulation in those who develop preclinical AD as assessed by a scalar cutoff. Critically, within cognitively normal individuals similar accumulation is absent in the group that remains PiB− at both time points but is present in those who became PiB+ at follow-up or who remained PiB+ at both time points. Evidence of Aβ pathology (e.g., in the CNnp group) is sufficient for classification as stage 1 preclinical AD (Jack et al., 2012; Sperling et al., 2011). Given that these participants became PiB + over a 3-year interval, this group represents the very earliest identifiable stages of preclinical AD. One method of operationalizing these criteria is through a scalar cutoff applied to some mean PiB binding index (Mintun et al., 2006). This is a potentially clinically useful method for summarizing the data and is predictive of eventual symptomatic conversion (Morris et al., 2009). However, the baseline MC SUVR failed to strongly correlate with future changes in MC SUVR, limiting its utility in early disease stages. In contrast, the multivariate topography, not restricted to regions typically involved in the late stages of AD, strongly correlated with change in MC SUVR in a penalized regression analysis. Overall, these data demonstrate that accounting for the multivariate PiB topography may help to understand and characterize the development of AD pathology over the different stages of the disease.

The application of multivariate statistics to the study of PiB topographies allows for the investigation of novel neurobiology. Previous work using mass univariate approaches necessarily included a data reduction step, for example, averaging over many regions of interest. This approach is powerful when the relevant topography is known. However, in the earliest stages of preclinical AD the relevant topography is unknown. Canonical correlation and penalized regression consider the entire topography in a minimally biased manner to maximize explanatory power. In this report, the additional power resulting from considering the entire distribution is leveraged to describe the topography of PiB associated with conversion to preclinical AD. Importantly, the identified topography is distinct from the maximally effected topography in late stage AD.

A critical analytic decision in the analysis of PiB data is resolution at which the analysis should be conducted. Currently, 3 analytic strategies dominate the literature: analysis of (1) global PiB binding over the entire cortex, (2) composite PiB binding in an a priori topography, or (3) regional/voxelwise PiB binding. The first 2 approaches are strong data reduction approaches that have demonstrated utility for predicting future symptomatic conversion (Ma et al., 2014; Morris and Price, 2001) though regional analysis may offer diagnostic advantages (Aizenstein et al., 2008). The notable feature of both of these approaches is the definition of a region of interest a priori (the whole cortex in the case of the former, specific topographies in the case of the latter). However, the relevant topography where PiB deposition maximally occurs changes with disease progression (Villain et al., 2012); the topography that predicts symptomatic conversion may not be useful for detecting changes associated with earliest disease onset. Regional analyses allow for the flexibility to

identify novel topographies but can yield varied results owing to the increased number of degrees-of-freedom (Engler et al., 2006; Grimmer et al., 2010; Jack et al., 2009; Kadir et al., 2012; Rinne et al., 2010; Villemagne et al., 2011). The presently reported results make use of multivariate techniques well suited to compiling regional data into meaningful topographies. Application of such approaches is especially important when the topographies of interest are not known a priori.

The conversion from PiB− to PiB+ necessarily involves deposition of additional Aβ. That additional deposition is not haphazard but usually follows a stereotypical progression (Braak and Braak, 1997; Thal et al., 2002). We report on distinct processes using canonical correlation analysis. We find evidence of a local and distributed process. In the local process, regions with PiB deposition at baseline simply accumulate more PiB plaques by the follow-up scan. However, in the distributed process, PiB in a particular topography correlates with PiB deposition in a different topography. Specifically, this progression represents the well-documented spread of Aβ deposition from posterior regions to more anterior regions (Thal et al., 2002).

The penalized regression model identifies topography of PiB retention that correlates with future PiB accumulation, either total value or percent change. Critically, the summary scalar was not a strong correlate of future percent change in PiB burden. The regions with positive β values largely overlap with known areas of Aβ retention early in the disease (Thal et al., 2002). However, not all regions overlap with previously defined summary metrics used for operationalizing the PiB+ definition. Notably, the previous scalar metric was defined based on the observations in the symptomatic stage of AD and does not necessary reflect the spatial pattern of PiB deposition in early preclinical stage (Mintun et al., 2006). This may lead to a biased view of early PiB burden using the MC SUVR approach. The caudate nucleus deserves specific discussion. Although it is known that caudate develops Aβ deposits throughout the disease (Thal et al., 2002), it is not commonly noted as a prominent initial contributor to PiB topography in late onset AD (but see Kemppainen et al., 2007). Nevertheless, the caudate nucleus is identified in both penalized regression models. However, it has been noted that individuals with autosomal dominant AD have particularly intense PiB retention in the striatum (Klunk et al., 2007). The independent evidence from this study and the study of autosomal dominant AD suggests some important, or at least reliable, process may be ongoing in the striatum early in AD.

The penalized regression identified several regions which were negatively loaded in both regression models. The presence of these negatively loaded regions demonstrates that the Aβ topography associated with advancing disease is specific. That is, PiB binding alone is not sufficient but rather it must be deposited in the disease causing topography. Amyloid in negatively loaded regions does not contribute to early disease pathophysiology. Indeed, Aβ is only present in the primary motor and sensory cortices much later in the disease (Braak and Braak, 1997), likely after symptoms develop. This potentially reflects that participants who have PiB retention in the precentral gyrus are unlikely to be PiB− at baseline. Thus, negatively loaded regions may serve as control regions by accounting for binding that is not because of Aβ or AD-related processes, especially at early disease stages. The presence of a

negatively predictive region indicates that it is not simply high values of PiB retention that predict conversion to PiB+ status but rather PiB deposition in a specific topography.

Only a small number of participants converted from PiB− status to PiB+ status which limits the robustness of this study. Additionally, the definition of converter compared with nonconverter is based on crossing a PiB threshold. Although such thresholds have been demonstrated to be potentially clinically useful (Mintun et al., 2006; Morris et al., 2009), other choices for a cutoff may be equally valid. Regardless of the precise definition, the primary scientific points remain: local and distributed processes are involved in the conversion to preclinical AD and consideration of the entire multivariate Aβ topography identifies correlates of advancing Aβ accumulation. A related point pertains to the prognostic information related to individuals who remain PiB− for the duration of the study but accumulate more PiB than average. These individuals are likely at an increased risk for developing preclinical AD in the future but longer follow-up time is required.

In summary, this study identified canonical correlations between baseline and follow-up PiB topographies in patients who converted from PiB− to PiB+. Penalized regression identified a topography association with future Aβ accumulation. Future studies could validate these regression models for their predictive power.

Supplementary Material

Refer to Web version on PubMed Central for supplementary material.

Acknowledgments

The authors acknowledge NIH funding from grants P01AG026276 (John C. Morris), 1R01NR012657 (Beau M. Ances), 1R01NR012907 (Beau M. Ances), 1R01NR014449 (Beau M. Ances), 1R21MH099979 (Beau M. Ances), and 5PO1AG026276 (John C. Morris). Funding was also provided from the NSF from grant DMS 1300280 (John E. McCarthy) and the Alzheimer's Association NIRP-12-257747 (Beau M. Ances). Finally, the authors also acknowledge generous support from Fred Simmons and Olga Mohan and the Paula and Rodger O. Riney fund.

Appendix A. Supplementary data

Supplementary data associated with this article can be found, in the online version, at http://dx.doi.org/10.1016/j.neurobiolaging.2015.10.025.

References

Aizenstein HJ, Nebes RD, Saxton JA, Price JC, Mathis CA, Tsopelas ND, Ziolko SK, James JA, Snitz BE, Houck PR, Bi W, Cohen AD, Lopresti BJ, DeKosky ST, Halligan EM, Klunk WE. Frequent amyloid deposition without significant cognitive impairment among the elderly. Arch Neurol. 2008; 65:1509–1517. [PubMed: 19001171]

Braak H, Braak E. Frequency of stages of Alzheimer-related lesions in different age categories. Neurobiol Aging. 1997; 18:351–357. [PubMed: 9330961]

Braak H, Del Tredici K. Where, when, and in what form does sporadic Alzheimer's disease begin? Curr Opin Neurol. 2012; 25:708–714. [PubMed: 23160422]

Braak H, Thal DR, Ghebremedhin E, Tredici KD. Stages of the pathological process in Alzheimer disease: age categories from 1 to 100 years. J Neuropathol Exp Neurol. 2011; 70:960–969. [PubMed: 22002422]

Brier MR, Mitra A, McCarthy JE, Ances BM, Snyder AZ. Partial covariance based functional connectivity computation using Ledoit-Wolf covariance regularization. Neuroimage. 2015; 121:29–38. [PubMed: 26208872]

Engler H, Forsberg A, Almkvist O, Blomquist G, Larsson E, Savitcheva I, Wall A, Ringheim A, Langstrom B, Nordberg A. Two-year follow-up of amyloid deposition in patients with Alzheimer's disease. Brain. 2006; 129:2856–2866. [PubMed: 16854944]

Fischl B, Salat DH, Busa E, Albert M, Dieterich M, Haselgrove C, van der Kouwe A, Killiany R, Kennedy D, Klaveness S, Montillo A, Makris N, Rosen B, Dale AM. Whole brain segmentation: automated labeling of neuroanatomical structures in the human brain. Neuron. 2002; 33:341–355. [PubMed: 11832223]

Grimmer T, Tholen S, Yousefi BH, Alexopoulos P, Forschler A, Forstl H, Henriksen G, Klunk WE, Mathis CA, Perneczky R, Sorg C, Kurz A, Drzezga A. Progression of cerebral amyloid load is associated with the apolipoprotein E epsilon4 genotype in Alzheimer's disease. Biol Psychiatry. 2010; 68:879–884. [PubMed: 20598287]

Hardle, W., Simar, L. Applied Multivariate Statistical Analysis. Springer; Berlin: 2007.

Hastie, T., Tibshirani, R., Friedman, JH. The Elements of Statistical Learning: Data Mining, Inference, and Prediction: With 200 Full-color Illustrations. Springer; New York: 2001.

Hotelling H. Relations between two sets of variates. Biometrika. 1936; 28:321–377.

Jack CR Jr, Knopman DS, Jagust WJ, Petersen RC, Weiner MW, Aisen PS, Shaw LM, Vemuri P, Wiste HJ, Weigand SD, Lesnick TG, Pankratz VS, Donohue MC, Trojanowski JQ. Tracking pathophysiological processes in Alzheimer's disease: an updated hypothetical model of dynamic biomarkers. Lancet Neurol. 2013; 12:207–216. [PubMed: 23332364]

Jack CR Jr, Knopman DS, Weigand SD, Wiste HJ, Vemuri P, Lowe V, Kantarci K, Gunter JL, Senjem ML, Ivnik RJ, Roberts RO, Rocca WA, Boeve BF, Petersen RC. An operational approach to National Institute on Aging-Alzheimer's Association criteria for preclinical Alzheimer disease. Ann Neurol. 2012; 71:765–775. [PubMed: 22488240]

Jack CR Jr, Lowe VJ, Weigand SD, Wiste HJ, Senjem ML, Knopman DS, Shiung MM, Gunter JL, Boeve BF, Kemp BJ, Weiner M, Petersen RC, Alzheimer's Disease Neuroimaging Initiative. Serial PIB and MRI in normal, mild cognitive impairment and Alzheimer's disease: implications for sequence of pathological events in Alzheimer's disease. Brain. 2009; 132:1355–1365. [PubMed: 19339253]

Kadir A, Almkvist O, Forsberg A, Wall A, Engler H, Langstrom B, Nordberg A. Dynamic changes in PET amyloid and FDG imaging at different stages of Alzheimer's disease. Neurobiol Aging. 2012; 33:198.e1–198.e14.

Kemppainen NM, Aalto S, Wilson IA, Nagren K, Helin S, Bruck A, Oikonen V, Kailajarvi M, Scheinin M, Viitanen M, Parkkola R, Rinne JO. PET amyloid ligand [11C]PIB uptake is increased in mild cognitive impairment. Neurology. 2007; 68:1603–1606. [PubMed: 17485647]

Klunk WE, Engler H, Nordberg A, Wang Y, Blomqvist G, Holt DP, Bergstrom M, Savitcheva I, Huang GF, Estrada S, Ausen B, Debnath ML, Barletta J, Price JC, Sandell J, Lopresti BJ, Wall A, Koivisto P, Antoni G, Mathis CA, Langstrom B. Imaging brain amyloid in Alzheimer's disease with Pittsburgh Compound-B. Ann Neurol. 2004; 55:306–319. [PubMed: 14991808]

Klunk WE, Price JC, Mathis CA, Tsopelas ND, Lopresti BJ, Ziolko SK, Bi W, Hoge JA, Cohen AD, Ikonomovic MD, Saxton JA, Snitz BE, Pollen DA, Moonis M, Lippa CF, Swearer JM, Johnson KA, Rentz DM, Fischman AJ, Aizenstein HJ, DeKosky ST. Amyloid deposition begins in the striatum of presenilin-1 mutation carriers from two unrelated pedigrees. J Neurosci. 2007; 27:6174–6184. [PubMed: 17553989]

Ledoit O, Wolf M. Improved estimation of the covariance matrix of stock returns with an application to portfolio selection. J Empirical Finance. 2003; 10:603–621.

Ledoit O, Wolf M. A well-conditioned estimator for large-dimensional covariance matrices. J Multivariate Anal. 2004; 88:365–411.

Ma Y, Zhang S, Li J, Zheng DM, Guo Y, Feng J, Ren WD. Predictive accuracy of amyloid imaging for progression from mild cognitive impairment to Alzheimer disease with different lengths of follow-up: a meta-analysis [Corrected]. Medicine (Baltimore). 2014; 93:e150. [PubMed: 25501055]

Minka T. Automatic choice of dimensionality for PCA. NIPS. 2000; 13:598–604.

Mintun MA, Larossa GN, Sheline YI, Dence CS, Lee SY, Mach RH, Klunk WE, Mathis CA, DeKosky ST, Morris JC. [11C]PIB in a non-demented population: potential antecedent marker of Alzheimer disease. Neurology. 2006; 67:446–452. [PubMed: 16894106]

Morris JC. The Clinical Dementia Rating (CDR): current version and scoring rules. Neurology. 1993; 43:2412–2414.

Morris JC, Blennow K, Froelich L, Nordberg A, Soininen H, Waldemar G, Wahlund LO, Dubois B. Harmonized diagnostic criteria for Alzheimer's disease: recommendations. J Intern Med. 2014; 275:204–213. [PubMed: 24605805]

Morris JC, Price JL. Pathologic correlates of nondemented aging, mild cognitive impairment, and early-stage Alzheimer's disease. J Mol Neurosci. 2001; 17:101–118. [PubMed: 11816784]

Morris JC, Roe CM, Grant E, Head D, Storandt M, Goate A, Fagan A, Holtzman DM, Mintun M. Pittsburgh compound B imaging and prediction of progression from cognitive normality to symptomatic Alzheimer disease. Arch Neurol. 2009; 66:1469–1475. [PubMed: 20008650]

Morris JC, Roe CM, Xiong C, Fagan AM, Goate AM, Holtzman DM, Mintun MA. APOE predicts amyloid-beta but not tau Alzheimer pathology in cognitively normal aging. Ann Neurol. 2010; 67:122–131. [PubMed: 20186853]

Price JL, McKeel DW Jr, Buckles VD, Roe CM, Xiong C, Grundman M, Hansen LA, Petersen RC, Parisi JE, Dickson DW, Smith CD, Davis DG, Schmitt FA, Markesbery WR, Kaye J, Kurlan R, Hulette C, Kurland BF, Higdon R, Kukull W, Morris JC. Neuropathology of nondemented aging: presumptive evidence for preclinical Alzheimer disease. Neurobiol Aging. 2009; 30:1026–1036. [PubMed: 19376612]

Rinne JO, Brooks DJ, Rossor MN, Fox NC, Bullock R, Klunk WE, Mathis CA, Blennow K, Barakos J, Okello AA, Rodriguez Martinez de Liano S, Liu E, Koller M, Gregg KM, Schenk D, Black R, Grundman M. 11C-PiB PET assessment of change in fibrillar amyloid-beta load in patients with Alzheimer's disease treated with bapineuzumab: a phase 2, double-blind, placebo-controlled, ascending-dose study. Lancet Neurol. 2010; 9:363–372. [PubMed: 20189881]

Rousset OG, Ma Y, Evans AC. Correction for partial volume effects in PET: principle and validation. J Nucl Med. 1998; 39:904–911. [PubMed: 9591599]

Schafer J, Strimmer K. A shrinkage approach to large-scale covariance matrix estimation and implications for functional genomics. Stat Appl Genet Mol Biol. 2005; 4 Article32.

Sojkova J, Zhou Y, An Y, Kraut MA, Ferrucci L, Wong DF, Resnick SM. Longitudinal patterns of beta-amyloid deposition in nondemented older adults. Arch Neurol. 2011; 68:644–649. [PubMed: 21555640]

Sperling RA, Aisen PS, Beckett LA, Bennett DA, Craft S, Fagan AM, Iwatsubo T, Jack CR Jr, Kaye J, Montine TJ, Park DC, Reiman EM, Rowe CC, Siemers E, Stern Y, Yaffe K, Carrillo MC, Thies B, Morrison-Bogorad M, Wagster MV, Phelps CH. Toward defining the preclinical stages of Alzheimer's disease: recommendations from the National Institute on Aging-Alzheimer's Association workgroups on diagnostic guidelines for Alzheimer's disease. Alzheimers Dement. 2011; 7:280–292. [PubMed: 21514248]

Su Y, Blazey TM, Snyder AZ, Raichle ME, Marcus DS, Ances BM, Bateman RJ, Cairns NJ, Aldea P, Cash L, Christensen JJ, Friedrichsen K, Hornbeck RC, Farrar AM, Owen CJ, Mayeux R, Brickman AM, Klunk W, Price JC, Thompson PM, Ghetti B, Saykin AJ, Sperling RA, Johnson KA, Schofield PR, Buckles V, Morris JC, Benzinger TL. Partial volume correction in quantitative amyloid imaging. Neuroimage. 2014; 121:29–38.

Su Y, Blazey TM, Snyder AZ, Raichle ME, Marcus DS, Ances BM, Bateman RJ, Cairns NJ, Aldea P, Cash L, Christensen JJ, Friedrichsen K, Hornbeck RC, Farrar AM, Owen CJ, Mayeux R, Brickman AM, Klunk W, Price JC, Thompson PM, Ghetti B, Saykin AJ, Sperling RA, Johnson KA, Schofield PR, Buckles V, Morris JC, Benzinger TL, Dominantly Inherited Alzheimer Network. Partial volume correction in quantitative amyloid imaging. Neuroimage. 2015; 107:55–64. [PubMed: 25485714]

Su Y, D'Angelo GM, Vlassenko AG, Zhou G, Snyder AZ, Marcus DS, Blazey TM, Christensen JJ, Vora S, Morris JC, Mintun MA, Benzinger TL. Quantitative analysis of PiB-PET with FreeSurfer ROIs. PloS One. 2013; 8:e73377. [PubMed: 24223109]

Thal DR, Rub U, Orantes M, Braak H. Phases of Aβ deposition in the human brain and its relevance for the development of AD. Neurology. 2002; 58:1791–1800. [PubMed: 12084879]

Tibshirani R. Regression shrinkage and selection via the Lasso. J R Stat Soc Series B Stat Methodol. 1996; 58:267–288.

Villain N, Chetelat G, Grassiot B, Bourgeat P, Jones G, Ellis KA, Ames D, Martins RN, Eustache F, Salvado O, Masters CL, Rowe CC, Villemagne VL, Group AIBL Research. Regional dynamics of amyloid-beta deposition in healthy elderly, mild cognitive impairment and Alzheimer's disease: a voxelwise PiB-PET longitudinal study. Brain. 2012; 135:2126–2139. [PubMed: 22628162]

Villemagne VL, Pike KE, Chetelat G, Ellis KA, Mulligan RS, Bourgeat P, Ackermann U, Jones G, Szoeke C, Salvado O, Martins R, O'Keefe G, Mathis CA, Klunk WE, Ames D, Masters CL, Rowe CC. Longitudinal assessment of Aβ and cognition in aging and Alzheimer disease. Ann Neurol. 2011; 69:181–192. [PubMed: 21280088]

Vlassenko AG, Mintun MA, Xiong C, Sheline YI, Goate AM, Benzinger TL, Morris JC. Amyloid-beta plaque growth in cognitively normal adults: longitudinal [(11) C]Pittsburgh compound B data. Ann Neurol. 2011; 70:857–861. [PubMed: 22162065]

Zou H, Hastie T. Regularization and variable selection via the elastic net. J R Statist Soc B. 2005; 67:301–320.

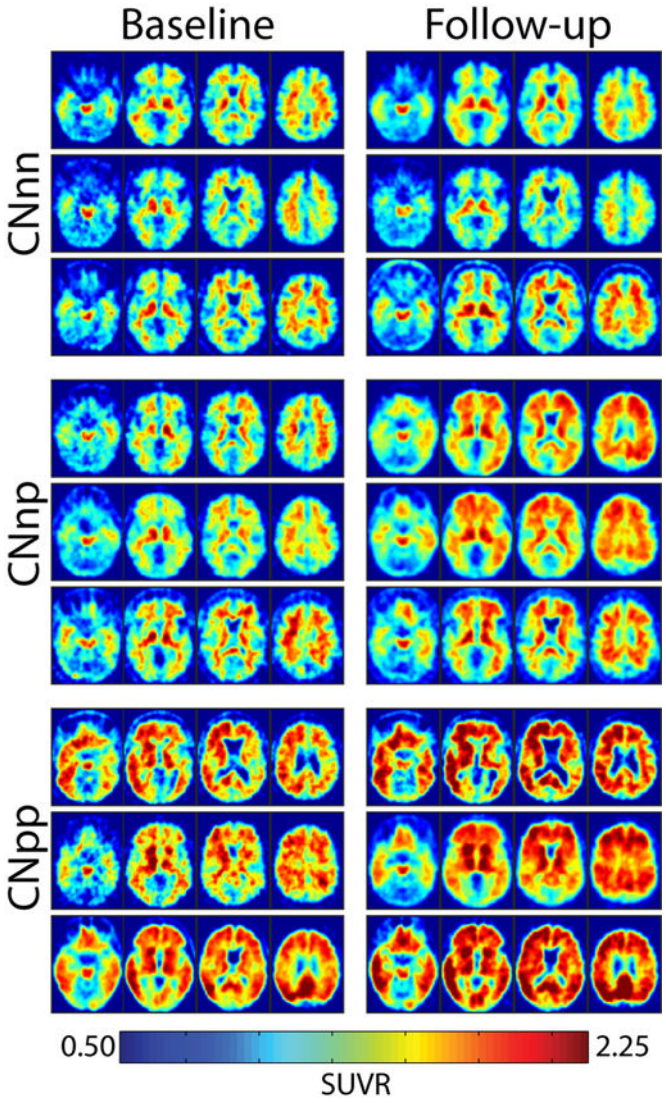

Fig. 1.

Baseline and follow-up SUVR images for the CNnn, CNnp, and CNpp group. Baseline and follow-up SUVR images for 3 randomly selected participants in each group. Abbreviations: CNnn, cognitively normal, PiB− at both scans; CNnp, cognitively normal, PiB− at first scan but PiB+ at second scan; CNpp, cognitively normal, PiB+ at both scans; SUVR, standardized uptake value ratio.

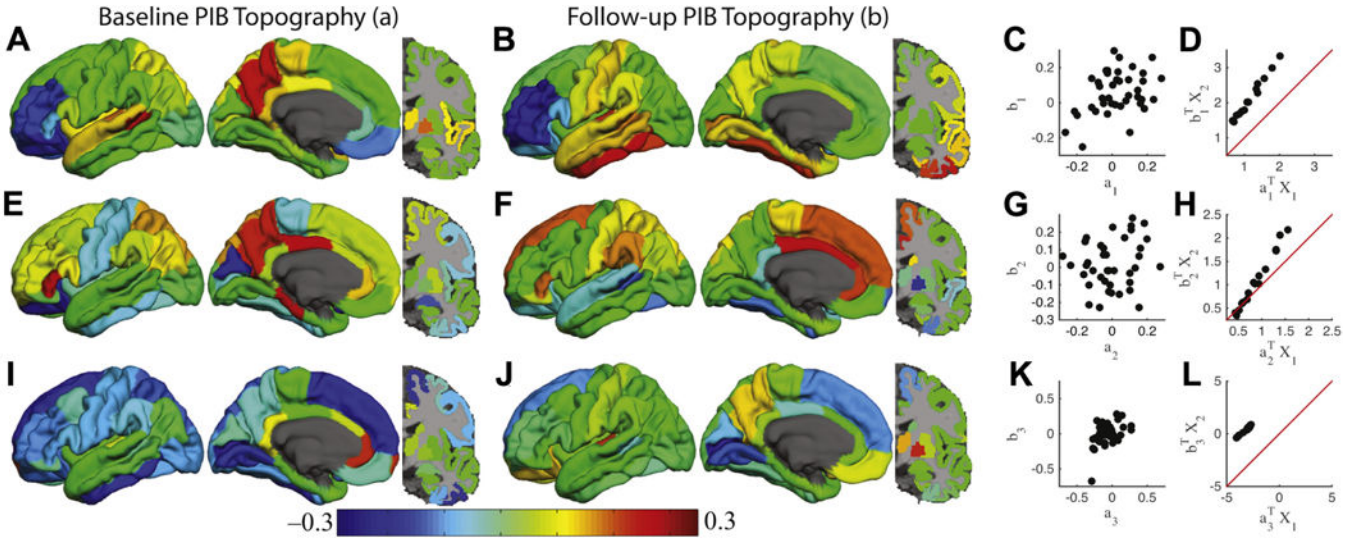

Fig. 2.

Canonical correlation analysis reveals distinct amyloid accumulation processes. The results corresponding to the first, second, and third canonical correlations are organized as individual rows. The first column (A, E, and I) shows the canonical variable (a) corresponding to the baseline PiB topography. The second column (B, F, and J) shows the canonical variable (b) corresponding to the follow-up PiB topography. These topographies are unit norm. The third column (C, G, and K) shows the correlation between the 2 canonical variables within a single canonical correlation. The fourth column (D, H, and L) shows the projection of the original data onto the canonical variables. Red line is the identity line. Abbreviation: PiB, Pittsburgh compound B. (For interpretation of the references to color in this figure legend, the reader is referred to the Web version of this article.)

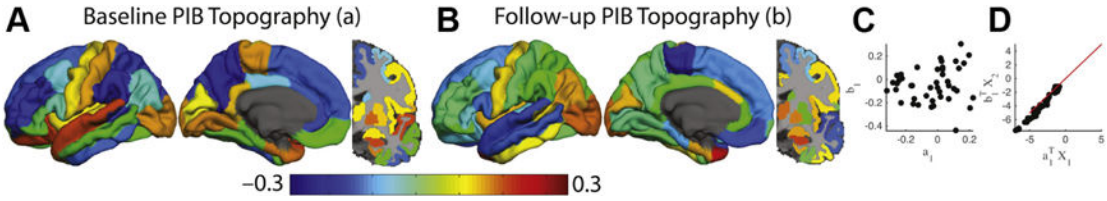

Fig. 3.

Canonical correlation analysis in the CNnn group reveals minimal amyloid accumulation. Canonical correlation analysis in the CNnn group using the same presentation style as Fig. 1 in the main text. (A) and (B) represent the maximally correlated baseline and follow-up topographies, respectively. (C) depicts the correlation between the two topographies. The critical feature here is that the correlated topographies do not exhibit marked accumulation (the data are along the identity line in D). Abbreviations: CNnn, cognitively normal, PiB− at both scans; PiB, Pittsburgh compound B.

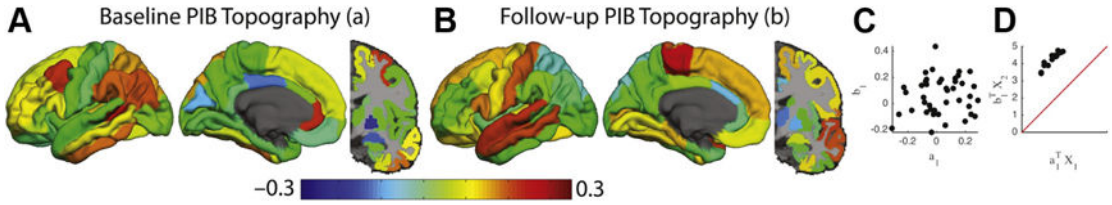

Fig. 4.

Canonical correlation analysis in the CNpp group reveals substantial amyloid accumulation. Canonical correlation analysis in the CNpp group using the same presentation style as Fig. 1 in the main text. (A) and (B) represent the maximally correlated baseline and follow-up topographies, respectively. (C) depicts the correlation between the two topographies. The critical feature here is that the correlated topographies exhibit marked accumulation (the data are above the identity line in D). Abbreviations: CNpp, cognitively normal, PiB+ at both scans; PiB, Pittsburgh compound B.

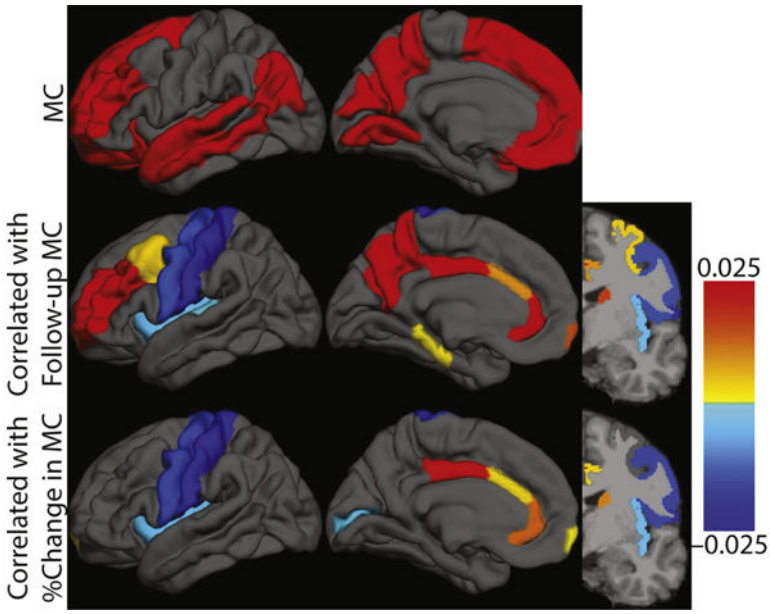

Fig. 5.

Topography of baseline Pittsburgh compound B deposition that correlates with follow-up and % change in mean cortical standardized uptake value ratio. Graphical representation of the information in Table 2. First row shows MC definition. Color bar indicates regression β values. Abbreviation: MC, mean cortical. (For interpretation of the references to color in this figure legend, the reader is referred to the Web version of this article.)

Table 1

Demographic information

Variable	CNnn	CNnp	CNpp	*p*
N	115	16	26	N/A
Age in y at baseline scan (SD)	59.5 (8.77)	66.4 (8.67)	68.2 (6.3)	<0.001
Gender (male/female)	35/80	5/11	10/16	0.73
Education in y (SD)	16.1 (2.4)	15.4 (2.5)	15.4 (2.4)	0.90
APOE ε4+ (% carriers)	23 (20)	9 (56)	17 (65)	<0.001
MC SUVR at baseline (SD)	0.97 (0.07)	1.17 (0.10)	2.12 (0.60)	<0.001
MC SUVR (follow-up)	1.02 (0.09)	1.47 (0.31)	2.48 (0.56)	<0.001
MMSE at baseline	29.3 (0.86)	29.3 (1.09)	28.9 (1.51)	0.73
MMSE at follow-up	29.4 (0.92)	29.4 (0.96)	29.0 (1.42)	0.89
Follow-up time in y (SD)	3.30 (1.45)	3.26 (1.20)	2.99 (1.26)	0.37

Mean (standard deviation) or counts for demographic variables.

Key: APOE ε4, apolipoprotein E ε4 positive indicates at least one APOE ε4 allele; CNnn, cognitively normal individuals, PiB negative at both scans; CNnp, cognitively normal, PiB-negative at first scan but PiB positive at second scan; MC SUVR, mean cortical standard uptake volume ratio of PiB deposition; MMSE, Mini-Mental Status Examination; SD, standard deviation.

Table 2

Elastic net regression coefficients

Region	Predictor Value	
	Follow-up MC SUVR	% Change in MC SUVR
Posterior cingulate	0.032	0.023
Rostral middle frontal	0.028	
Rostral anterior cingulate	0.027	0.014
Precuneus	0.025	
Baseline MC SUVR	0.021	
Caudate	0.017	0.011
Frontal pole	0.016	0.002
Caudal anterior cingulate	0.010	0.004
Caudal middle frontal	0.005	
Parahippocampal gyrus	0.003	
Pericalcerine		−0.003
Transverse temporal	−0.001	
Insula	−0.004	−0.004
Precentral gyrus	−0.015	−0.016
Postcentral gyrus	−0.027	−0.023

Table of penalized (elastic net) regression coefficients. Blank spaces correspond to coefficients equal to zero.

Key: MC SUVR, mean cortical standard uptake volume ratio.